# Supporting Information

Lambert et al. 10.1073/pnas.0912934107
Supporting Information Corrected January 26, 2012

## SI Materials and Methods

**Single Turnover GTPase Assays.** Mutations of Gly-321 to alanine in the *S. cerevisiae* Gpa1 cDNA and Gly-202 to alanine in the human $G\alpha_{i1}$ cDNA were separately achieved using QuikChange site-directed mutagenesis (Stratagene). Mutant or wild-type Gα protein (100 nM) was incubated at 30 °C for 15 min in buffer C (50 mM Tris, pH 7.5, 0.05% $C_{12}E_{10}$, 1 mM DTT, 5 mg/mL BSA, 10 mM EDTA, 100 mM NaCl) containing ~$1 \times 10^6$ cpm of [γ-$^{32}$P]GTP (6,000 Ci/mmol). Samples were then placed on ice for 5 min. GTPase reactions (on ice) were initiated by adding 10 mM $MgCl_2$ (with 100 mM GTPγS to ensure measuring a single round of GTP hydrolysis), and timed reaction aliquots were quenched by charcoal slurry (containing 20 mM $H_3PO_4$, pH 3) followed by centrifugation (~4,000 × *g* for 10 min at 4 °C). Supernatants containing free [$^{32}$P] inorganic phosphate were analyzed by scintillation counting. Background counts (in the absence of Gα) were subtracted from all experimental conditions.

**Crystal Growth and Structure Determinations.** Crystals of $G\alpha_{i1}$-(G202A) protein (in GDP form) were grown using the hanging drop method in which 4 μL of protein was mixed 1:1 with 4 μL of buffer (1.8~2.2 M ammonium sulfate, 100 mM sodium acetate, pH 5.5~6.5). Crystals formed in 2–4 days at 18°C. The GDP-bound protein crystallized in the space group I4 (a = b = 120.5 Å, c = 68.2 Å; α = β = γ = 90°) with 1 molecule in the asymmetric unit. Crystals were cryoprotected in crystallization buffer supplemented with 20% glycerol for ~1 min and submerged in liquid $N_2$. Native data sets of 2.34 Å (GDP form) were collected at the UNC-Chapel Hill Biomolecular x-ray Crystallography Facility using an R-Axis-IV$^{++}$ beamline. Data were scaled and indexed using HKL-2000 (1). The structure of wild-type $G\alpha_{i1}$·GDP (PDB id 1GDD; ref (2).), excluding waters and GDP, was used for molecular replacement (3). Model building was completed using Coot (4) and O (5), with successive rounds of simulated annealing, minimization, B-group, and rigid body refinements being completed by CNS (6). All electron density map calculations were completed with CNS. All structural images were generated using PyMol (DeLano Scientific) unless otherwise denoted.

**Surface Plasmon Resonance–Based Assay of the Gα·GDP/Gβγ Interaction.** Wild-type and G202A mutant $His_6$-$G\alpha_{i1}$ proteins were purified as described previously in the main text except that, after Ni-NTA chromatography, protein fractions were pooled and resolved on a calibrated Superdex S200 gel filtration column equilibrated with Hepes pH 7.5 (50 mM), NaCl (150 mM), GDP (10 μM), and glycerol (2.5% vol/vol). Surface plasmon resonance-based measurements of $G\alpha_{i1}$·GDP binding were performed on a Biacore 3000 (GE Healthcare) at room temperature using separate streptavidin biosensors (Sensor Chip SA) containing either 500 or 800 response units (RUs) of immobilized, biotinylated $G\beta_1\gamma_1$ (ref. 7), or 800 RUs of biotinylated $G\alpha_{i1}$ (8) as a negative control surface (i.e., Gα subunits do not dimerize). Before injection over biosensor surfaces, $G\alpha_{i1}$ proteins were diluted in Biacore running buffer of 10 mM Hepes pH 7.4, 150 mM NaCl, and 0.005% (vol/vol) Nonidet P-40. Injections were performed using the KINJECT command with an injection volume of 200 μL and a dissociation time of 300 seconds at a flow rate of 20 μL/min. Bulk changes in refractive index were subtracted in BiaEvaluation software (GE Healthcare) using sensorgram curves derived from the nonspecific binding surface. Dose–response curves were subsequently plotted from the normalized binding observed at equilibrium (590 s after injection start; $n = 2$ for each dose) vs. Gα concentration; nonlinear regression was performed to determine apparent affinities ($K_d$ values) and their standard error using GraphPad Prism v.5.0c.

**Yeast Strains and Plasmids.** The yeast *S. cerevisiae* strain used in this study was BY4741 (*MAT***a** *leu2Δ met15Δ his3-1 ura3Δ*), in combination with yeast shuttle plasmids pRS406 (amp$^R$, *URA3*) and pRS423 *FUS1*-lacZ. Gpa1 point mutants were integrated into BY4741 cells using the pRS406 integrating vector; by inserting truncated *gpa1* lacking the promoter region and the start codon, it was possible to simultaneously insert the mutant *gpa1* and knock out the wild-type GPA1 gene. The pRS406 GPA1$^{81-1538bp}$ plasmid was constructed by PCR amplification of *GPA1* from genomic DNA with forward primer 5′-TA*T CTA GA*C GAG CAA TCG TTG CAG CTG G-3′ (containing an XbaI site) and reverse primer 5′-CAT AGC ATC GAT CCA TCA TAG ACT CTA ATG G-3′ (containing a ClaI site). The PCR product was cloned into the XbaI/ClaI sites of the pRS406 multicloning region. Genomic integration of Gpa1$^{81-1538bp}$ used linearization via an unique HindIII site in the *gpa1* open-reading frame downstream of both the G302S and the G321A point mutations. These two point mutations were created using QuikChange site-directed mutagenesis (Stratagene): G302S using mutagenic primer 5′-GCC GTA TAA AGA CTA CAA GCA TTA CAG AAA CCG-3′ and its reverse complement, and G321A using mutagenic primer 5′-GGT TCT CGA CGC TGC TGG GCA GCG TTC TGA ACG-3′ and its reverse complement.

Correct genomic integration of mutants was assayed by PCR. The forward primer was designed to terminate on the signal base-pair substitution of the mutant gene: G302S mutant detection primer was 5′-GGG CCG TAT AAA GAC TAC AA-3′ and the G321A mutant detection primer was 5′-TTC AAG GTT CTC GAC GCT GC-3′. Amplification of a PCR product using the mutant detection primers, and a lack of a PCR product using wild-type primers, was indicative of integration of the mutant *gpa1*.

**Pheromone Transcriptional Reporter Assays.** Yeast cells were grown to $A_{600nm}$ ~0.8 and treated with α-factor pheromone for 90 min before addition of a fluorescein di-β-galactopyranoside (FDG) solution (final concentrations: 83 nM FDG, 0.04% Triton X-100, 21.6 mM Pipes, pH 7.2) and further incubation in the dark at 37 °C for 60 min. Reaction was stopped by the addition of $Na_2CO_3$ to a final concentration of 143 mM, and fluorescence at 485–530 nm was measured with a VersaMax optical plate reader (Molecular Devices). Data were analyzed with Prism (GraphPad Software) and dose–response curves fit via nonlinear regression analysis (sigmoidal dose–response, variable slope).

**Halo Assay of Pheromone-Induced Growth Inhibition.** Yeast cells were grown to saturation in liquid medium, diluted (1:400) into 4 mL of 0.5% (wt/vol) dissolved agar (50 °C), and then spread onto culture plates of the same medium. Sterile filter discs were spotted with recombinant α-factor peptide (3, 1, 0.3, and 0.1 μg) and placed onto the freshly spread lawn of yeast cells. The resulting zone of growth inhibition was measured after 2 days incubation at 30 °C.

**Plasmid DNA Constructs for Mammalian Expression.** The Gβγ BRET sensor masGRKct-Rluc8 contained amino acids G495-L688 of bovine GRK3 (NP_776925; a.k.a. β-adrenergic receptor kinase 2

or βARK2), preceded by a myristic acid attachment peptide (mas; MGSSKSKTSNS). The stop codon of GRK3 was replaced with a GGG linker, which was followed by the *Renilla reniformis* luciferase variant Rluc8 (9). The original masGRK3 construct was a generous gift from Stephen R. Ikeda (National Institute on Alcohol Abuse and Alcoholism, Rockville, MD). $G\beta_1\gamma_2$-V was expressed by cotransfecting plasmids encoding amino acids 1–155 of the fluorescent protein Venus fused to a GGSGGG linker and the N terminus of human $G\gamma_2$ (Venus1-155-$G\gamma_2$) and amino acids 156–239 of Venus fused to a GGSGGG linker and the N terminus of human $G\beta_1$ (Venus155-239-$G\beta_1$) (10). RGS insensitivity (G184S) and switch-II fast hydrolysis (G203A) mutations were introduced into PTX-insensitive (C351G) human $G\alpha_{oA}$. All constructs were made using an adaptation of the QuikChange (Stratagene) mutagenesis protocol, were expressed from pcDNA3.1 (Invitrogen), and were verified by automated sequencing.

**Mammalian Cell Culture and Transfection.** HEK 293 cells (ATCC) were propagated in plastic flasks according to the supplier's protocol. Cells were transfected using linear polyethyleneimine (MW 25,000; Polysciences Inc) at an N/P ratio of 20; up to 3 μg of plasmid DNA was transfected per well of a six-well plate. Cells were used for experiments 12–24 h after transfection. Human $D_2$ dopamine receptors (D2Rs), Gα, Gβ, Gγ, and GRK plasmids were transfected at a 1:2:1:1:1 ratio, and PTX (100 ng·mL$^{-1}$; List Biologicals) was added to the culture medium immediately after transfection.

**BRET Measurements and Curve Fitting.** Cells were detached from plates by rinsing with PBS-EDTA and triturating in PBS. Suspended cells were transferred to black 96-well microplates (Nunc, Thermo Scientific) and benzyl-coelenterazine (coelenterazine h; 5 μM; Nanolight Technologies) was added to all wells immediately before making measurements. Luminescence measurements were made using a photon-counting multimode plate reader (Mithras LB940; Berthold Technologies). The raw BRET signal (em535/480) was calculated as the emission intensity at 520–545 nm divided by emission intensity at 475–495 nm. Net BRET was this ratio minus the same ratio measured from cells expressing only the BRET donor (Rluc8). Data points were generally collected every 0.6 s, although a subset of experiments was performed with data points collected every 0.1 s. Raw data points were fitted to a single exponential function using the method of least squares and the Levenberg-Marquardt algorithm. Fitted curves were judged as adequate when the coefficient of determination ($R^2$) was >0.8. Curve fitting was performed to provide an objective estimate of response onset and recovery kinetics, even in cases when it was clear that more than a single process governed the time course (e.g., acute response desensitization with rapid hydrolysis; Fig. 3*B*).

**BRET-Based Assessment of RGS Domain/Gα Mutant Interactions.** Venus was fused to the C terminus of rat RGS8 with a GGG linker. Rluc8 flanked by GGGG linkers was fused to the various $G\alpha_{oA}$ mutants internally between amino acids 91 and 92. Cells expressing these constructs were exposed to either PBS or PBS with 10 mM $MgCl_2$, 60 μM $AlCl_3$, and 10 mM NaF (to form aluminum tetrafluoride).


1. Otwinowski Z, Minor W (1997) Processing of X-ray diffraction data collected in oscillation mode. *Methods Enzymol* 276:307–326.
2. Mixon MB, et al. (1995) Tertiary and quaternary structural changes in Gi alpha 1 induced by GTP hydrolysis. *Science* 270:954–960.
3. Navaza J (2001) Implementation of molecular replacement in AMoRe. *Acta Crystallogr D Biol Crystallogr* 57:1367–1372.
4. Emsley P, Cowtan K (2004) Coot: Model-building tools for molecular graphics. *Acta Crystallogr D Biol Crystallogr* 60:2126–2132.
5. Jones TA, Zou JY, Cowan SW, Kjeldgaard M (1991) Improved methods for building protein models in electron density maps and the location of errors in these models. *Acta Crystallogr A* 47:110–119.
6. Brünger AT, et al. (1998) Crystallography & NMR system: A new software suite for macromolecular structure determination. *Acta Crystallogr D Biol Crystallogr* 54:905–921.
7. Johnston CA, et al. (2008) Structural determinants underlying the temperature-sensitive nature of a Galpha mutant in asymmetric cell division of Caenorhabditis elegans. *J Biol Chem* 283:21550–21558.
8. Willard FS, Low AB, McCudden CR, Siderovski DP (2007) Differential G-alpha interaction capacities of the GoLoco motifs in Rap GTPase activating proteins. *Cell Signal* 19:428–438.
9. Loening AM, Fenn TD, Gambhir SS (2007) Crystal structures of the luciferase and green fluorescent protein from Renilla reniformis. *J Mol Biol* 374:1017–1028.
10. Hynes TR, et al. (2004) Visualization of G protein betagamma dimers using bimolecular fluorescence complementation demonstrates roles for both beta and gamma in subcellular targeting. *J Biol Chem* 279:30279–30286.

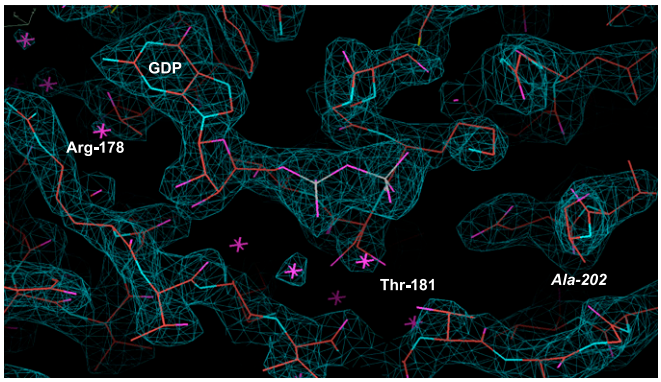


**Fig. S1.** Electron density representation of the final model of $G\alpha_{i1}$(G202A) bound to GDP, highlighting the bound nucleotide, the $G\alpha_{i1}$ residues Arg-178 and Thr-181 of switch-I, and the mutant alanine (in italics) of switch-II at residue position 202. Experimental electron density is shown as a 2Fo-Fc simulated annealing composite omit map contoured at 1σ (electron density shown as blue mesh). Ordered waters are highlighted with purple asterisks. Image was generated in Coot.

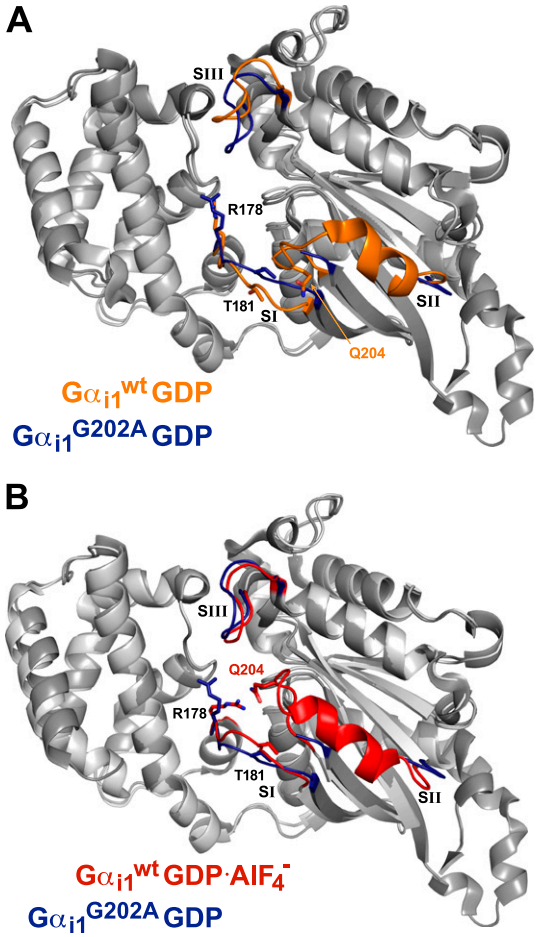


**Fig. S2.** Comparisons of the structural models of wild-type $G\alpha_{i1}$ in its inactive (GDP-bound; *A*) and transition-state mimetic ($GDP{\cdot}AlF_4^-$-bound; *B*) forms, with the $G\alpha_{i1}$ G202A mutant, highlighting dispositions of the three switch regions (SI, SII, and SIII) and the key catalytic residues Arg-178, Thr-181, and Gln-204. Structural models were derived from PDB records: 1GP2 (*orange*), wild-type $G\alpha_{i1}{\cdot}GDP$ (within the $G\alpha\beta\gamma$ heterotrimer complex which leads to ordered switch regions *vs* the disorder seen with isolated, wild-type $G\alpha_{i1}{\cdot}GDP$); 1GF1 (red), wild-type $G\alpha_{i1}{\cdot}GDP{\cdot}AlF_4^-$; and, 3UMS (blue), $G\alpha_{i1}$(G202A)·GDP.

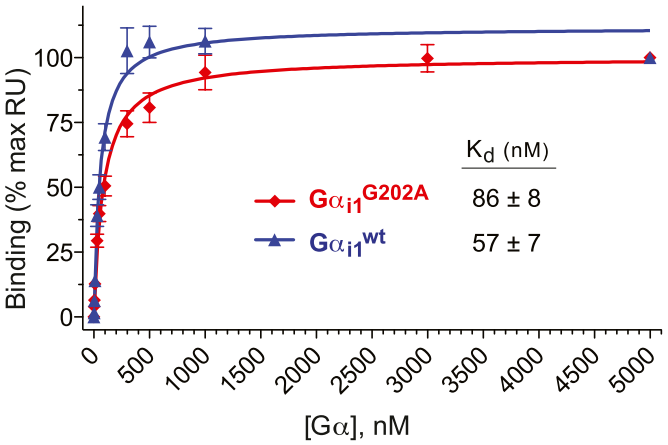


**Fig. S3.** The G202A mutation does not dramatically alter the affinity of Gα·GDP for Gβγ. Wild-type $G\alpha_{i1}$·GDP and $G\alpha_{i1}$(G202A)·GDP (at indicated concentrations) were separately injected over immobilized, biotinylated $G\beta_1\gamma_1$ biosensor surfaces. Surface plasmon resonance (SPR) responses achieved at equilibrium binding were normalized to maximal resonance unit (RU) responses and plotted vs. Gα concentration. Resultant $B_{max}$ curves were fit by nonlinear regression to obtain dissociation constant ($K_d$) values which are presented with standard error (GraphPad Prism) (*Inset*).

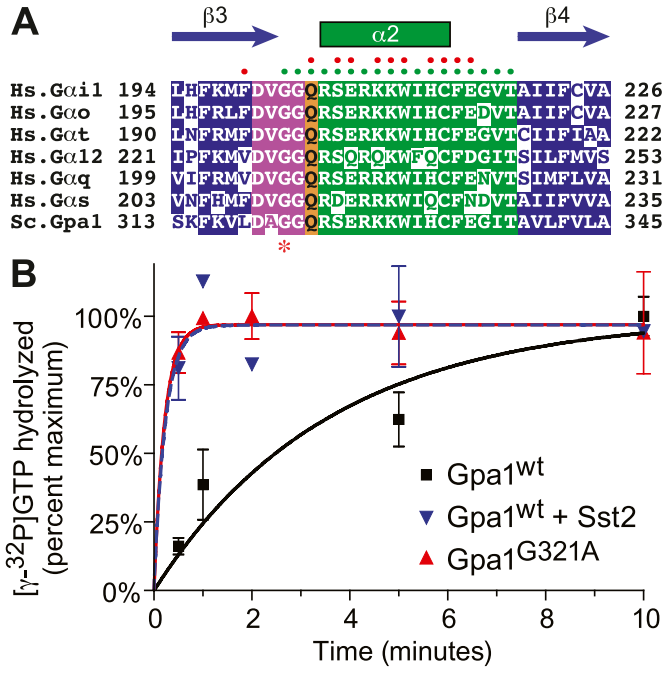


**Fig. S4.** The fast-hydrolysis glycine-to-alanine switch II mutation is transferable to *S. cerevisiae* Gpa1. (*A*) Alignment of human $G\alpha_{i1}$ (GenBank AAM12619) and *S. cerevisiae* Gpa1 (GenBank NP011868) highlighting conservation of switch II residues (green dots), including Gly-202 of $G\alpha_{i1}$ (Gly-321 of Gpa1; red asterisk). Secondary structure and colored highlights of conserved nucleotide contacts (magenta), GTPase catalytic residues (orange), and Gβ contact residues (red dots) follow those of Johnston and Siderovski (1). (*B*) Single-turnover GTP hydrolysis data demonstrating enhanced intrinsic GTPase rate of Gpa1(G321A). Purified Gα protein (100 nM) was loaded with [$\gamma$-$^{32}$P]GTP (~$1 \times 10^6$ cpm) for 15 min at 30 °C in the absence of $Mg^{2+}$, followed by 5 min incubation on ice. Baseline aliquots were removed and $MgCl_2$ (10 mM)–containing buffer, with or without the RGS domain of Sst2 (aa 420–689), was added to initiate reactions. Aliquots were taken at indicated timepoints and analyzed for [$^{32}$P]Pi content as previously described (2). Calculated GTPase rates were as follows: Gpa1(wt): 0.28 $min^{-1}$; Gpa1 (wt) + Sst2(RGS domain): 4.2 $min^{-1}$; Gpa1(G321A): 4.6 $min^{-1}$.

1. Johnston CA, Siderovski DP (2007) Receptor-mediated activation of heterotrimeric G-proteins: current structural insights. *Mol Pharmacol* 72:219–230.
2. Afshar K, et al. (2004) RIC-8 is required for GPR-1/2-dependent Galpha function during asymmetric division of C. elegans embryos. *Cell* 119:219–230.

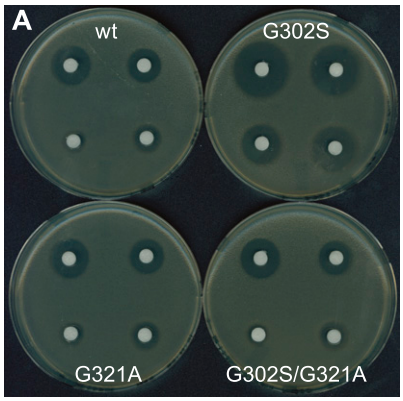


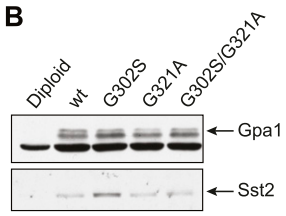


C

| Gpa1 | Halo length (mm) | $EC_{50}$ (μM) | Hill slope | Max. response (%wt) |
|---|---|---|---|---|
| wildtype (wt) | 21 | 2.07 ± 0.08 | 2.1 ± 0.1 | 100 |
| G302S (RGS-i) | 29 | 0.26 ± 0.02 | 1.1 ± 0.1 | 83.5 ± 1.4 |
| G321A (fast GTPase) | 21 | 1.98 ± 0.07 | 2.2 ± 0.1 | 80.5 ± 1.0 |
| G302S/G321A | 21 | 1.82 ± 0.06 | 2.2 ± 0.1 | 86.2 ± 1.1 |

**Fig. S5.** $Gpa1^{G321A}$ restores proper pheromone signaling to RGS-insensitive yeast. Strain BY4741 of *S. cerevisiae* was transformed with integrating plasmids (pRS406) containing $Gpa1^{WT}$, $Gpa1^{G302S}$, $Gpa1^{G321A}$, or $Gpa1^{G302S/G321A}$. (*A*) Yeast were plated onto solid medium and exposed to paper discs containing α-factor (counterclockwise starting from bottom left: 0.1, 0.3, 1.0, and 3.0 μg) for 48 h. (*B*) To ensure equal expression of the integrated *Gpa1* gene locus in all four strains, yeast grown to midlog phase were collected and fractionated/resolved by 10% SDS/PAGE for immunoblotting using anti-Gpa1 antibodies and anti-Sst2 antibodies. Diploid yeast that do not express Gpa1 or Sst2 served as a negative control (first lane). The nonspecific protein band below Gpa1 was used to determine equal loading. (*C*) Quantification of the halo formation and transcriptional response and assays on the indicated haploid yeast strains. Halo length represents the diameter of the halo for the highest concentration of pheromone tested (3.0 μg). A 50% effective dose ($EC_{50}$) and Hill slope values were derived from measured transcriptional responses over 11 different pheromone concentrations subjected to nonlinear regression analysis (sigmoidal dose–response, variable slope).

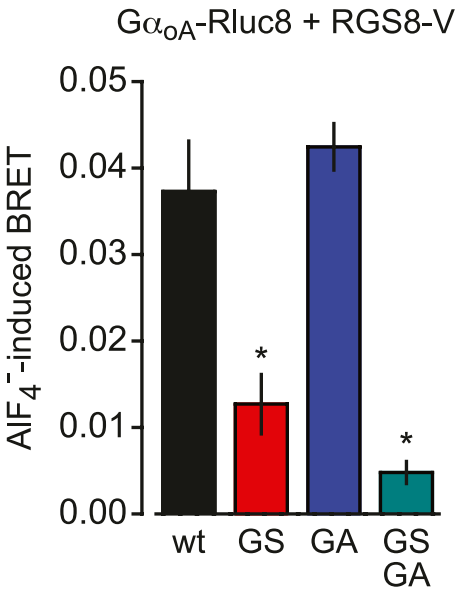


**Fig. S6.** Aluminum tetrafluoride ($AlF_4^-$)–induced BRET signal was observed to be significantly greater for wild-type $G\alpha_{oA}$ ("wt") and the fast-hydrolysis G203A ("GA") mutant of $G\alpha_{oA}$, compared with the RGS-insensitive G184S-containing $G\alpha_{oA}$ mutants ($n = 5$ in quadruplicate; $P < 0.001$, one-way ANOVA with Bonferroni means comparison).

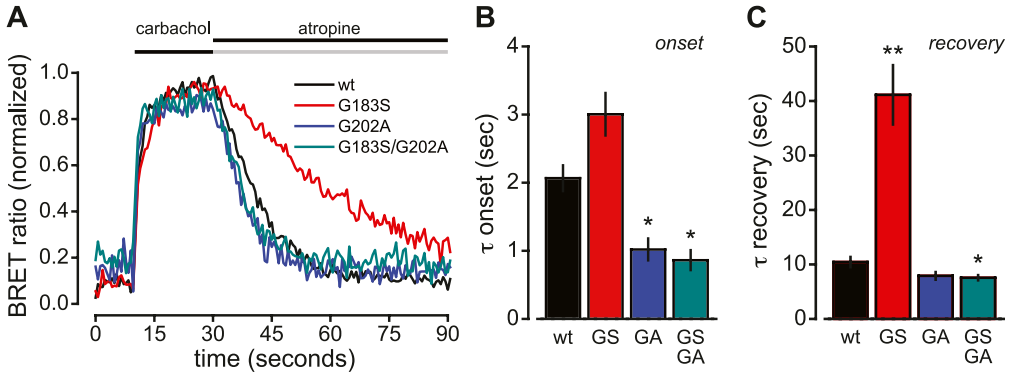


**Fig. S7.** The glycine-to-alanine switch II mutation G202A restores rapid onset and recovery kinetics to responses of the M4 muscarinic acetylcholine receptor as mediated by RGS-insensitive $G\alpha_{i1}$ in HEK 293 cells. (*A*) Normalized BRET between masGRKct-Rluc8 and $G\beta_1\gamma_2$-V is plotted against time during sequential addition of carbachol (30 μM) and atropine (100 μM) for each of the four $G\alpha_{i1}$ variants indicated (all pertussis-toxin insensitive). Traces represent the mean of three experiments, each performed in quadruplicate. (*B*) Average onset time constants plotted for each of the four $G\alpha_{i1}$ variants (± SEM, $n = 5$). (*C*) Average recovery time constants plotted for each of the four $G\alpha_{i1}$ variants (± SEM, $n = 3$, performed in quadruplicate); $^*P < 0.05$, $^{**}P < 0.01$ vs. wt.

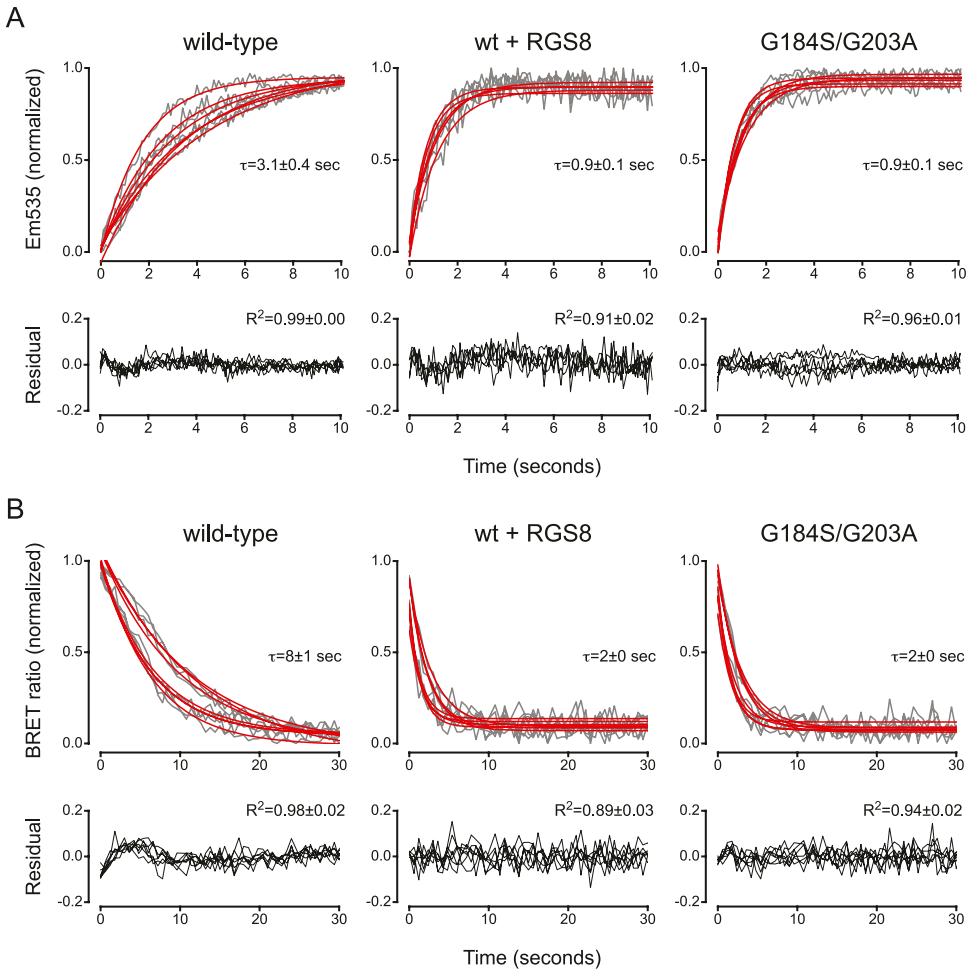


**Fig. S8.** Examples of single exponential curves fitted by the method of least squares. (*A*) Onset phases mediated by D2R and the indicated $G\alpha_{oA}$ subunits were fitted to a single exponential function; the agonist quinpirole was added at time = 0; ($n = 6$). In these experiments only a single wavelength (355 nm) was monitored to allow data points to be acquired every 0.1 s. (*B*) Recovery phases; haloperidol was added at time = 0 to cells that had been pretreated with quinpirole ($n = 6$). In these experiments, the BRET ratio was monitored every 0.6 s. Derived mean onset and recovery time constants (τ) and $R^2$ for these six experiments (±SEM) are given.

**Table S1. Data collection and refinement statistics for $G\alpha_{i1}$(G202A) crystal structure**

| | $G\alpha_{i1}$(G202A)·GDP PDB id 3UMS |
|---|---|
| Data collection | |
| Space group | I4 |
| Unit cell dimensions *a, b, c* (Å) | 120.5, 120.5, 67.9 |
| α, β, γ (°) | 90, 90, 90 |
| Resolution range (Å) | 31.58 – 2.34 (2.36 – 2.34) |
| No. of unique reflections | 19,799/344 |
| $R_{merge}$ | 0.071 (0.898) |
| Mean //σ | 27.7 (2.0) |
| Completeness (%) | 94.5 (67.4) |
| Redundancy | 4.2 (3.9) |
| Wilson B value (Å$^2$) | 55.0 |
| Refinement | |
| Resolution (Å) | 31.58 – 2.34 |
| No. of reflections (working/test set) | 18,609/1,183 |
| $R_{work}/R_{free}$ (%) | 18.0/22.8 |
| No. of atoms (non-hydrogen): | |
| Protein | 2,696 |
| GDP/$SO_4^{2-}$/$Cl^-$ | 28/5/1 |
| Waters | 130 |
| Average B-factor (Å$^2$) | |
| Protein | 52.4 |
| GDP/$SO_4^{2-}$/$Cl^-$ | 33.5/ 54.0/ 86.8 |
| Waters | 46.5 |
| R.m.s. deviations: | |
| Bonds (Å) | 0.008 |
| Angles (°) | 1.078 |
| Ramachandran plot (% in region): | |
| Allowed | 97.0 |
| Generously allowed | 3.0 |
| Disallowed | 0.0 |

Numbers in parentheses pertain to the highest-resolution shell.

**Table S2. Signal onset and recovery data as measured in this study and those of Saitoh et al. (1) and Doupnik et al. (2), along with effective concentration at 50% maximum ($EC_{50}$) and the maximum agonist-induced response divided by the maximum response in the presence of GTPγS ($R_{max}$; e.g., Fig. 3C)**

| Receptor system | $\tau_{onset}$ (s) | $\tau_{recov}$ (s) | $EC_{50}$ (M) | $R_{max}$ |
|---|---|---|---|---|
| D2R $G\alpha_{oA}$ wt | 1.8 | 7.5 | $4.1 \times 10^{-7}$ | 0.69 |
| D2R $G\alpha_{oA}$ G184S | 3.0 | 31.9 | $9.0 \times 10^{-8}$ | 0.75 |
| D2R $G\alpha_{oA}$ G203A | 0.8 | 2.9 | $4.9 \times 10^{-7}$ | 0.51 |
| D2R $G\alpha_{oA}$ wt + RGS8 | 0.9 | 1.9 | $2.4 \times 10^{-6}$ | 0.35 |
| D2R $G\alpha_{oA}$ GS/GA | 0.8 | 2.1 | $1.2 \times 10^{-6}$ | 0.44 |
| M4R $G\alpha_{i1}$ wt | 2.07 | 10.43 | $5.1 \times 10^{-7}$ | 0.81 |
| M4R $G\alpha_{i1}$ G183S | 3.00 | 41.13 | $2.0 \times 10^{-7}$ | 0.89 |
| M4R $G\alpha_{i1}$ G202A | 1.02 | 7.91 | $2.8 \times 10^{-7}$ | 0.89 |
| M4R $G\alpha_{i1}$ GS/GA | 0.86 | 7.56 | $1.3 \times 10^{-7}$ | 0.86 |
| (Saitoh) D2R -RGS8 | 2.91 | 12.76 | $6.7 \times 10^{-7}$ | |
| (Saitoh) D2R +RGS8 | 1.10 | 4.71 | $1.0 \times 10^{-6}$ | |
| (Saitoh) M2R -RGS8 | 6.02 | 11.36 | $2.1 \times 10^{-7}$ | |
| (Saitoh) M2R +RGS8 | 1.19 | 3.91 | $2.5 \times 10^{-7}$ | |
| (Doupnik) M2R -RGS4 | 1.40 | 21.00 | $\sim 50 \times 10^{-9}$ | |
| (Doupnik) M2R +RGS4 | 0.60 | 5.00 | $\sim 50 \times 10^{-9}$ | |


1. Saitoh O, Kubo Y, Miyatani Y, Asano T, Nakata H (1997) RGS8 accelerates G-protein-mediated modulation of K+ currents. *Nature* 390:525–529.
2. Doupnik CA, Davidson N, Lester HA, Kofuji P (1997) RGS proteins reconstitute the rapid gating kinetics of gbetagamma-activated inwardly rectifying K+ channels. *Proc Natl Acad Sci USA* 94:10461–10466.